

Article

# A Nonlinear Inverse Design Problem for a Pipe Type Heat Exchanger Equipped with Internal Z-Shape Lateral Fins and Ribs

Cheng-Hung Huang \* and Chih-Yang Kuo

Department of Systems and Naval Mechatronic Engineering, National Cheng Kung University, Tainan 701, Taiwan; kevin851011001@gmail.com

\* Correspondence: chhuang@mail.ncku.edu.tw

Received: 12 November 2020; Accepted: 2 December 2020; Published: 4 December 2020



**Abstract:** A non-linear three-dimensional inverse shape design problem was investigated for a pipe type heat exchanger to estimate the design variables of continuous lateral ribs on internal Z-shape lateral fins for maximum thermal performance factor  $\eta$ . The design variables were considered as the positions, heights, and number of ribs while the physical properties of air were considered as a polynomial function of temperature; this makes the problem non-linear. The direct problem was solved using software package CFD-ACE+, and the Levenberg–Marquardt method (LMM) was utilized as the optimization tool because it has been proven to be a powerful algorithm for solving inverse problems. Z-shape lateral fins were found to be the best thermal performance among Z-shape, S-shape, and V-shape lateral fins. The objective of this study was to include continuous lateral ribs to Z-shape lateral fins to further improve  $\eta$ . Firstly, the numerical solutions of direct problem were solved using both polynomial and constant air properties and then compared with the corrected solutions to verify the necessity for using polynomial air properties. Then, four design cases, A, B, C and D, based on various design variables were conducted numerically, and the resultant  $\eta$  values were computed and compared. The results revealed that considering continuous lateral ribs on the surface of Z-shape lateral fins can indeed improve  $\eta$  value at the design working condition  $Re = 5000$ .  $\eta$  values of designs A, B and C were approximately 13% higher than that for Z-shape lateral fins, however, when the rib numbers were increased, i.e., design D, the value of  $\eta$  became only 11.5 % higher. This implies that more ribs will not guarantee higher  $\eta$  value.

**Keywords:** nonlinear shape design problem; pipe type heat exchanger; Levenberg–Marquardt method; Z-shape lateral fins with ribs

## 1. Introduction

It is well known that if a furnace produced industrial waste heat that can be recycled by utilizing economizers or regenerators before it is discharged into the environment, the thermal efficiency of the system can thus be improved significantly. In addition, if the exhaust gas can be cooled down to a reasonably low temperature before its discharge then this will also be environmentally friendly.

Economizers and regenerators are basically the so-called pipe type heat exchangers, and internally longitudinal finned tubes are usually utilized to effectively enhance heat transfer for the tube side. They can be used in many practical industrial applications such as petroleum industries, boiler systems, power plants and chemical engineering industries.

Many researchers have investigated the research topic regarding internally longitudinal finned tubes problems. For instance, Webb [1] has discussed internally finned tubes in detail, and Fabbri [2,3] examined an optimal design problem in determining the lateral profile of longitudinal fins located in cylindrical tubes.

The pressure drop behaviors inside circular finned tubes under turbulent flow conditions were examined experimentally by El-Sayed et al. [4]. They have reported that, in the periodic fully developed region, the tube pressure drop with continuous fins is higher than that of inline arrangement fins and lower than that of staggered arrangement fins. The heat transfer performance of vertical internally finned tube under forced convection condition were investigated numerically by Al-Sarkh and Abu-Nada [5]. They have found the existence of an optimum combination of fin numbers and height to yield the best heat transfer performance.

Heat transfer performance of a three-dimensional heat exchanger with internally longitudinally finned tube with blocked core tube and stream wise wavy fin was examined numerically by Wang et al. [6]. The numerical solutions were verified by comparing them with the experimental data and the effects of both wave height and wave distance on heat transfer performance were investigated. The numerical results indicated that the Nusselt number and friction factor increase with the increase in the wave height, while they decrease with the increase in the wave distance. Yu and Tao [7] investigated the pressure drop and heat transfer characteristics of turbulent flow in annular tubes with internal wave-like longitudinal fins. Results revealed that heat transfer can be enhanced using wave-like finned tubes and wave number 20 can result in best performance.

Three different lateral fin profiles, i.e., S-shape, Z-shape and V-shape, of internally finned tubes with blocked core-tube was investigated and the heat transfer performances of those lateral fin profiles were examined by Wang et al. [8]. The hydro-thermal performances of the studied lateral fin profiles were computed and compared under three working conditions. It was found that Z-shape fins have the best performance.

Based on the research findings in Wang et al. [8], Duan et al. [9] extended the concept of Z-shape fins to construct the blossom shape internal fins and utilized in a double-tube structure internally finned tube. The hydro-thermal behaviors of the heat exchanger were analyzed, and the conclusion was that the blossom shape fin is more suitable for the exhaust gas heat recovery system than the wave-like fin.

Rib-roughened cooling passages are commonly used in heat exchangers; the utilization of ribs on the fin surface of heat exchanger introduces two heat transfer enhancement characteristics, i.e., an increase in heat transfer area and a significant increase in heat transfer coefficients.

Much research regarding this topic can be found in the open literature. For example, Chai et al. [10] numerically investigated the thermal performance of a microchannel heat sink with rectangular inserted ribs. They have considered the designs with different rib lengths and widths and arrangements, and concluded that when  $Re < 600$ , the interrupted microchannel with ribs was a good passive method for heat transfer enhancement. Xia et al. [11] studied the micro heat sink equipped with fan-shaped reentrant cavities and internal ribs. Result indicated that the effect of rib height was stronger than the individual effect of the size or arrangement of the reentrant cavity for  $Re > 300$ .

Ahmed [12] investigated the optimal design of a ribbed flat-plate fin heat sink. In this work, the sizes, positions, numbers, and orientations of ribs were considered as the design variables and the objective was to obtain the optimal thermal performance heat sink. Results indicated that a ribbed plate fin heat sink provides thermal performance of 1.55 times greater than a plate fin heat sink under the studied conditions.

Based on the above preliminary reviews, it is expected that the thermal performance factor of a pipe type heat exchanger can be improved by including continuous lateral ribs to internal Z-shape lateral fins. The objective of this shape design problem is to determine the optimal sizes and number of continuous lateral ribs to yield the optimal thermal performance factor under fixed fin volume constraints with an efficient optimization tool.

The Levenberg–Marquardt method (LMM) [13] has been considered as an efficient optimization tool for shape design problems. For instance, Chen and Huang [14] used LMM and commercial code SHIPFLOW to estimate the optimal shape of the after hull based on the desired wake distribution. Huang and Li [15] determined the optimal boundary geometry of a three-dimensional conductive

body for producing boundary isotherms with LMM. Huang and Chen [16] used LMM to estimate the optimal shape and perforation diameters of a perforated pin-fin array module. A three-dimensional wavy-shaped fin array design problem was considered by Huang and Tung [17], and the objective was to estimate the optimal wavy-shaped fin array with deformed sinusoidal function to minimize the average temperature of the base plate of fin array under a fixed fin volume constraint. Therefore, LMM was chosen in this study as the optimization algorithm.

## 2. Problem Formulation

A 3-D Pipe Type Heat Exchanger with blocked core-tube and internal Z-shape lateral fins with ribs (PTHE-ZR) was studied in the present inverse design problem to illustrate the methodology for estimating the optimal design variables of lateral ribs using LMM and CFD-ACE+ [18].

Figure 1 indicates the physical model of PTHE with internal Z-type lateral fins (PTHE-Z) listed with the parameter index. PTHE-Z is composed of an annulus tube and Z-shape lateral fins, the tube length is 400 mm, and there are 20 waves located in the cross-section of internally finned tube. The diameters are considered as  $d_o = 16$  mm,  $D_i = 32$  mm,  $D_o = 35$  mm and  $\delta = 0.2$  mm,  $t = 0.1$  mm,  $L = 7.6$  mm,  $L_t = 400$  mm, and  $N = 20$ . The inlet air temperature and wall temperature are taken as  $T_{in} = 373$  K and  $T_w = 303$  K, respectively [9], inlet pressure is considered as  $P_{in} = 0.2$  MPa, and thermal conductivity of copper is  $k_{copper} = 387$  W/m-K.

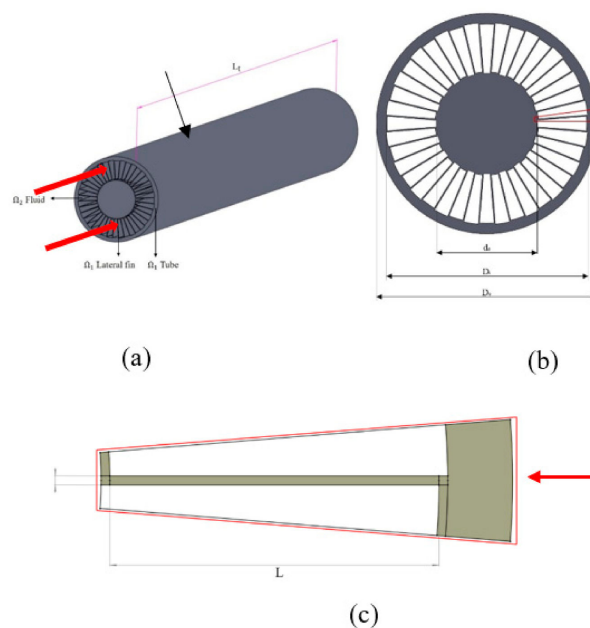


**Figure 1.** The physical model of PTHE-Z. (a) three-dimensional view, (b) cross-sectional view and (c) computational region.

Here,  $\Omega$  represents the computational domain and  $\{\Omega\} = \{\Omega_1 \cup \Omega_2\}$ , where  $\Omega_1$  indicates the solid regions (tube and Z-shape lateral fin materials) and  $\Omega_2$  is the working air flow region. The outer boundary surfaces of PTHE are subjected to constant wall temperature boundary conditions.

Due to the axial symmetry of PTHE-Z, for simplicity of computations, the computational domain is chosen as 1/40 of the original PTHE-Z and its 3-D computational domain and grid system are given in Figure 2a,b, respectively.

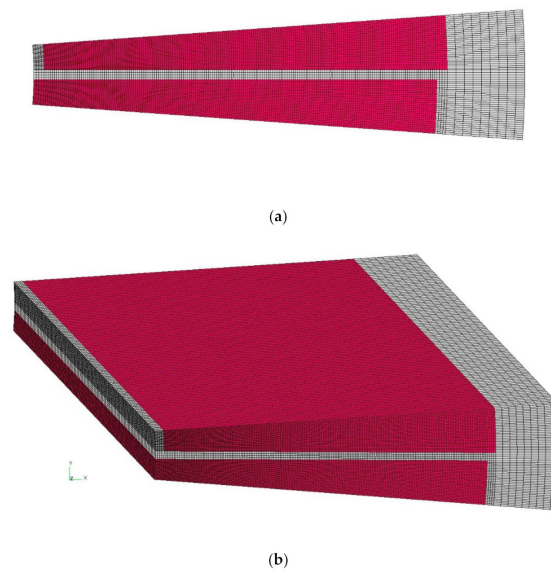


**Figure 2.** Grid system: (a) cross-sectional view and (b) three-dimensional view.

The conduction equation for the 3-D solid domain  $\Omega_1$  is given by:

$$\left[ \frac{\partial^2 T_s(\Omega_1)}{\partial x^2} + \frac{\partial^2 T_s(\Omega_1)}{\partial y^2} + \frac{\partial^2 T_s(\Omega_1)}{\partial z^2} \right] = 0; \text{ in } \Omega_1 \quad (1)$$

where  $T_s$  represents the solid, i.e., tube and fin, material temperature distributions in  $\Omega_1$ .

It is assumed that air is a 3-D steady-state incompressible flow in region  $\Omega_2$  and the thermal properties of air are assumed to be a function of temperature; this makes the problem non-linear. In addition, due to force convection and moderate air temperature conditions, buoyancy and radiative heat transfer effects are both neglected.

The 3-D equations of continuity, momentum, and energy in the steady-state turbulent flow with the standard  $k$ - $\varepsilon$  model, turbulent kinetic energy and turbulent energy dissipation rate are illustrated in Equations (2)–(6), respectively [19]:

$$\frac{\partial \rho u_i}{\partial x_i} = 0 \quad (2)$$

$$\frac{\partial \rho u_j u_i}{\partial x_j} = -\frac{\partial p}{\partial x_i} + \frac{\partial}{\partial x_j} \left[ \mu_t \left( \frac{\partial u_i}{\partial x_j} + \frac{\partial u_j}{\partial x_i} \right) \right] \quad (3)$$

$$\frac{\partial \rho u_j T_a}{\partial x_j} = \frac{\partial}{\partial x_j} \left[ \left( \frac{\mu_1}{\sigma_1} + \frac{\mu_t}{\sigma_t} \right) \frac{\partial T_a}{\partial x_j} \right] \quad (4)$$

$$\frac{\partial \rho u_j k}{\partial x_j} = \frac{\partial}{\partial x_j} \left( \frac{\mu_t}{\sigma_k} \frac{\partial k}{\partial x_j} \right) + \mu_t \left( \frac{\partial u_i}{\partial x_j} + \frac{\partial u_j}{\partial x_i} \right) \frac{\partial u_i}{\partial x_j} - \rho \varepsilon \quad (5)$$

$$\frac{\partial \rho u_j \varepsilon}{\partial x_j} = \frac{\partial}{\partial x_j} \left( \frac{\mu_t}{\sigma_\varepsilon} \frac{\partial \varepsilon}{\partial x_j} \right) + C_1 \mu_t \frac{\varepsilon}{k} \left( \frac{\partial u_i}{\partial x_j} + \frac{\partial u_j}{\partial x_i} \right) \frac{\partial u_i}{\partial x_j} - C_2 \rho \frac{\varepsilon^2}{k} \quad (6)$$

where  $\mu_1$  and  $\mu_t$  are the kinematic viscosity and turbulent viscosity, respectively, and  $\sigma_1$  and  $\sigma_t$  stand for the kinematic Schmidt number and turbulent Schmidt number, respectively, with  $\mu_t = C_\mu (k^2/\varepsilon)$ ,  $C_1 = 1.44$ ,  $C_2 = 1.92$ ,  $C_\mu = 0.09$ ,  $\sigma_k = 1.0$  and  $\sigma_\varepsilon = 1.3$ .  $T_a$  represents air temperature distribution in  $\Omega_2$ . It is assumed a non-slip boundary condition, i.e.,  $u_i = 0$ , applied on all pipe surfaces. The 3-D hydro-thermal conjugate problem in domain  $\Omega$  of PTHE-Z is solved using CFD-ACE+, and the physical properties of air are assumed as a function of air temperature  $T_a$ .

The functions of density  $\rho(T_a)$ , specific heat  $C_p(T_a)$ , viscosity  $\mu_l(T_a)$  and conductivity  $k_a(T_a)$  of air are given below [9]:

$$\rho(T_a) = 6 \times 10^{-6} \times (T_a - 273)^2 - 0.0058 \times (T_a - 273) + 2.4028 \text{ (kg/m}^3\text{)} \quad (7)$$

$$C_p(T_a) = -3 \times 10^{-9} \times (T_a - 273)^3 + 2 \times 10^{-6} \times (T_a - 273)^2 - 0.0001 \times (T_a - 273) + 1.004 \text{ (kJ/kg} \cdot \text{K)} \quad (8)$$

$$\mu_l(T_a) = 1 \times 10^{-6} \times (T_a - 273)^3 - 0.0007 \times (T_a - 273)^2 + 0.1679 \times (T_a - 273) + 10.282 \text{ (kg/m} \cdot \text{s)} \quad (9)$$

$$k_a(T_a) = 3 \times 10^{-6} \times (T_a - 273)^2 + 0.0084 \times (T_a - 273) + 2.3802 \text{ (W/m} \cdot \text{K)} \quad (10)$$

Equations (7)–(10) indicate that the values of thermal properties depend on the value of  $T_a$ , and this makes the problem nonlinear. Equations (1)–(10) are utilized to calculate the pressure, velocity and temperature distributions for PTHE-Z when all the boundary conditions and the size of the internal Z-shape lateral fins are known. Thereafter, the average outlet air temperature  $T_{out}$  can be calculated.

The Reynolds number  $Re$ , Nusselt number  $Nu$ , and friction factor  $f$  are defined as follows:

$$Re = \frac{\rho u_{in} D_h}{\mu_l} \quad (11)$$

$$Nu = \frac{h D_h}{k_a} \quad (12)$$

$$f = \frac{\Delta P}{(\rho u^2 / 2)(L_t / D_h)} \quad (13)$$

where  $u_{in}$  and  $\Delta p$  are the inlet velocity and total pressure drop, respectively,  $D_h$  denotes hydraulic diameter and is defined clearly in [8], and  $L_t$  is the tube length with internal fins. In addition, the heat transfer coefficient  $h$  is defined as:

$$h = \frac{\dot{m} C_p (T_{in} - T_{out})}{A \Delta T_{LMTD}} \quad (14)$$

In Equation (14),  $A$  denotes the total heat transfer area, and  $\Delta T_{LMTD}$  represents the logarithmic mean temperature difference and is defined as:

$$\Delta T_{LMTD} = \frac{(T_{in} - T_w) - (T_{out} - T_w)}{\ln\left(\frac{T_{in} - T_w}{T_{out} - T_w}\right)} \quad (15)$$

Here,  $T_{in}$  and  $T_{out}$  represent the inlet and average outlet air temperatures of heat exchanger, respectively, and  $T_w$  is the tube wall temperature. Based on the constant pumping power constraint, the thermal performance factor  $\eta$  of PTHE-ZR is defined as the ratio between the convective heat transfer coefficients of PTHE-ZR,  $h_{ZR}$ , and PTHE-Z,  $h_Z$ . Finally,  $\eta$  of PTHE-ZR can be obtained below [20,21]:

$$\eta = \left(\frac{h_{ZR}}{h_Z}\right)_{pp} = \left(\frac{Nu_{ZR}}{Nu_Z}\right)_{pp} = \left(\frac{Nu_{ZR}}{Nu_Z}\right) \left(\frac{f_{ZR}}{f_Z}\right)^{-\frac{1}{3}} \quad (16)$$

Under identical power conditions,  $\eta \geq 1$  indicates that the increase in the enhancement ratio of heat transfer rate ( $Nu_{ZR}/Nu_Z$ ) is larger than the increase in friction losses ( $f_{ZR}/f_Z$ )<sup>-1/3</sup>. A higher  $\eta$  will result in better heat dissipation performance under the same energy consumption conditions.

### 3. The Inverse Design Problem of Ribs

Wang et al. [8] utilized a  $k-\varepsilon$  turbulence model with a wall function method to investigate the hydro-thermal performance of PTHE with internal lateral fins and blocked core-tube. PTHE with S-shape, Z-shape, and V-shape internally lateral fin profiles, i.e., PTHE-S, PTHE-Z and PTHE-V, were investigated and compared. They have concluded that PTHE-Z achieved the best hydro-thermal performance.

It is well known that roughness elements such as ribs can be used on heat exchanger surfaces to promote turbulence and enhance convective heat transfer. These various types of ribs are mounted on fin surfaces and have been widely used in engineering applications to enhance heat transfer of heat exchangers, mixing chambers, turbine blade cooling and electronic equipment cooling.

The design concept of this study was to include some pairs of rectangular lateral ribs on the surface of Z-shape fin to improve the thermal performance factor  $\eta$  of PTHE-ZR.

The proper design variables need be identified prior to the design process, and only effective design variables need to be included to avoid the long computational time of the design process. The following four design cases will be considered and investigated.

#### 3.1. Design A

In design A, it is assumed that there is one pair of rib and the position  $W$  and height  $H$  of rib are considered as the design variables. Figure 3a–c indicates the geometry of the isometric view, cross-sectional view, and computational domain of PTHE-ZR, respectively. The design variables  $W$  and  $H$  can be rearranged in the following expression:

$$\Theta = \{\Theta_1, \Theta_2\} = \{W, H\} \quad (17)$$

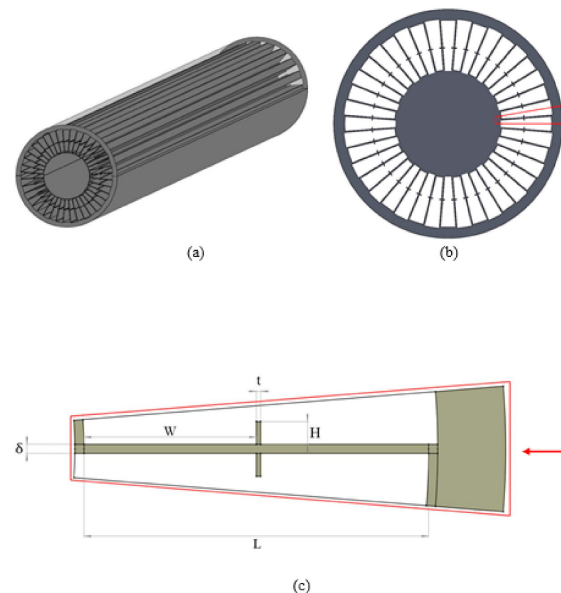


**Figure 3.** The physical model of design A PTHE-ZR. (a) three-dimensional view, (b) cross-sectional view and (c) computational region.

Figure 3 implies that the fin position and height of upper and lower ribs are identical. In addition, the volume of each lateral fin with ribs,  $Vol$ , is obtainable using the following equation:

$$Vol = (L \times \delta + 2 \times H \times t) \times L_t \quad (18)$$

Once  $H$  is determined, the thickness of lateral fin  $\delta$  can be obtained using volume constraint condition Equation (18) and the geometry of Figure 3c can be constructed.

### 3.2. Design B

In design B, it is also assumed that there is one pair of ribs, however, the position  $W_1$  and the height  $H_1$  of the upper rib, and the position  $W_2$  and the height  $H_2$  of the lower rib are considered as the design variables. Figure 4a–c indicates the geometry of the isometric view, cross-sectional view, and computational domain of PTHE-ZR, respectively. The design variables  $W_1$ ,  $W_2$ ,  $H_1$  and  $H_2$  are arranged as follows:

$$\Theta = \{\Theta_1, \Theta_2, \Theta_3, \Theta_4\} = \{W_1, H_1, W_2, H_2\} \quad (19)$$

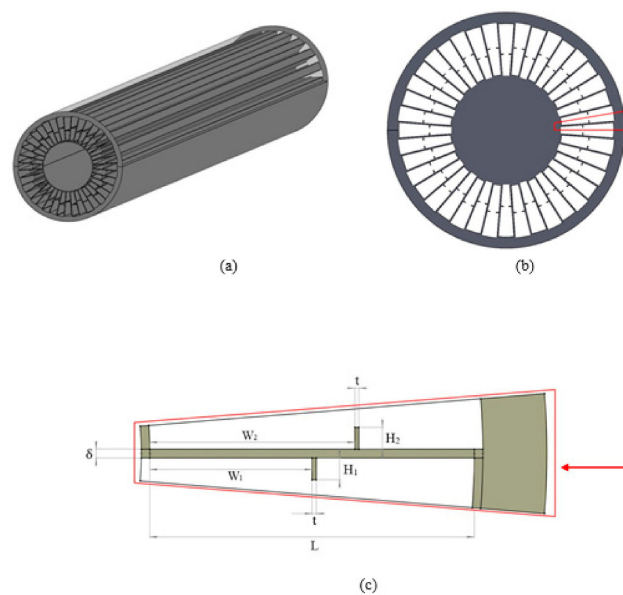


**Figure 4.** The physical model of design B PTHE-ZR. (a) three-dimensional view, (b) cross-sectional view and (c) computational region.

Figure 4c indicates that there are four design variables in design B. The volume of each lateral fin with ribs,  $Vol$ , can be computed with the equation below:

$$Vol = [L \times \delta + (H_1 + H_2) \times t] \times L_t \quad (20)$$

Once  $H_1$  and  $H_2$  are obtained, the thickness of the lateral fin  $\delta$  can be computed from Equation (20) and the geometry of PTHE-ZR can then be plotted.

### 3.3. Design C

In design C, two pairs of ribs are considered and Figure 5a–c plots the geometry of the isometric view, cross-sectional view, and computational domain of the PTHE-ZR in design C, respectively. It can be learned from Figure 5c that the positions  $W_1$  and  $W_2$  and the heights  $H_1$  and  $H_2$  of ribs are considered as the design variables, i.e., there are also four design variables in design C.

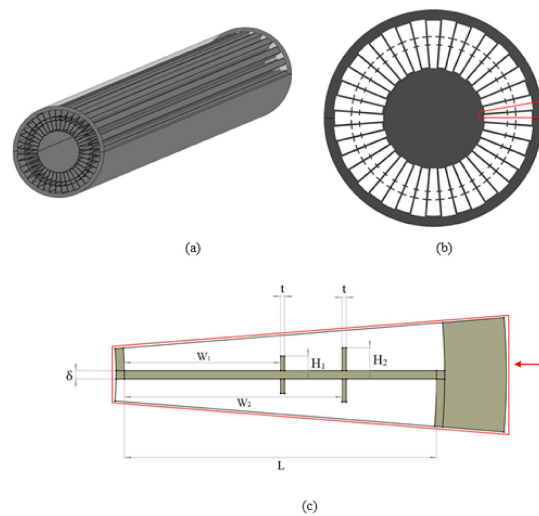


**Figure 5.** The physical model of design C PTHE-ZR. (a) three-dimensional view, (b) cross-sectional view and (c) computational region.

The design variables  $W_1$ ,  $W_2$ ,  $H_1$  and  $H_2$  are arranged as follows:

$$\Theta = \{\Theta_1, \Theta_2, \Theta_3, \Theta_4\} = \{W_1, H_1, W_2, H_2\} \quad (21)$$

The volume of each lateral fin with ribs, Vol, can be calculated using the following expression:

$$\text{Vol} = [L \times \delta + 2 \times (H_1 + H_2) \times t] \times L_t \quad (22)$$

Once  $H_1$  and  $H_2$  are obtained, the thickness of the lateral fin  $\delta$  can be obtained using Equation (22) and the geometry of PTHE-ZR in design C can be plotted.

### 3.4. Design D

Three pairs of ribs are considered in design D, and Figure 6a–c illustrates the geometry of the isometric view, cross-sectional view, and computational domain of PTHE-ZR in design D, respectively. It is clear that the positions  $W_1$ ,  $W_2$ , and  $W_3$  and the heights  $H_1$ ,  $H_2$ , and  $H_3$  of ribs are considered as the design variables, i.e., there are six design variables in design D.

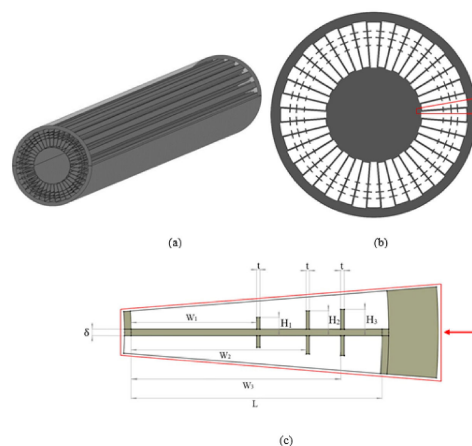


**Figure 6.** The physical model of design D PTHE-ZR. (a) three-dimensional view, (b) cross-sectional view and (c) computational region.

The design variables  $W_1, W_2, W_3, H_1, H_2$  and  $H_3$  can be arranged as follows:

$$\Theta = \{\Theta_1, \Theta_2, \Theta_3, \Theta_4, \Theta_5, \Theta_6\} = \{W_1, H_1, W_2, H_2, W_3, H_3\} \quad (23)$$

The volume of each lateral fin with ribs, Vol, can be calculated using the following expression:

$$\text{Vol} = [L \times \delta + 2 \times (H_1 + H_2 + H_3) \times t] \times L_t \quad (24)$$

Once  $H_1, H_2$  and  $H_3$  are estimated, the thickness of lateral fin  $\delta$  can be obtained using Equation (24) and the geometry of PTHE-ZR in design D can be plotted.

### 3.5. The Cost Function

The purpose of this work was to obtain the optimal value of  $\eta(\Theta)$  by determining the optimal shape of PTHE-ZR. Letting the desired  $\eta(\Theta)$  of PTHE-ZR be denoted as  $\phi$ , the fin shape design problem can be stated as follows: utilize  $\phi$  to design PTHE-ZR for yielding optimal thermal performance factor  $\eta(\Theta)$ .

The cost function of the present shape design problem is as follows:

$$J[\Omega(\Theta)] = [\eta(\Theta) - \phi]^2 = \mathbf{A}^T \mathbf{A} \quad (25)$$

Here,  $\Omega$  denotes the computational domain of the PTHE-ZR and is a function of the design variable  $\Theta$ .  $\eta$  denotes the estimated thermal performance factor of PTHE-ZR, and its value is calculated from the solution of the direct problem by using an updated geometry of PTHE-ZR. In addition, the volume constraints, Equations (18), (20), (22) and (24) for designs A, B, C and D, must be satisfied.

## 4. The Optimization Algorithm

The cost function is minimized with respect to the design variable  $\Theta$  to obtain the following equation:

$$\frac{\partial J[\Omega(\Theta)]}{\partial \Theta} = \left[ \frac{\partial \eta(\Theta)}{\partial \Theta} \right] [\eta - \phi] = 0 \quad (26)$$

Equation (26) is linearized by expanding  $\eta(\Theta)$  in a Taylor series and retaining only the first-order terms. Thereafter, a weighting coefficient  $\mu^n$  is included in the resultant expression to speed up the rate of convergence. Finally, the Levenberg–Marquardt method [13] can be obtained as:

$$(\mathbf{F} + \mu^n \mathbf{I}) \Delta \Theta = \mathbf{D} \quad (27)$$

$$\mathbf{F} = \Psi^T \Psi \quad (28)$$

$$\mathbf{D} = \Psi^T \mathbf{A} \quad (29)$$

$$\Delta \Theta = \Theta^{n+1} - \Theta^n \quad (30)$$

Here,  $\mathbf{I}$  denotes the identity matrix, the superscripts T and n represent the transpose matrix and iteration index, respectively, and  $\Psi$  is the Jacobian matrix and is given as:

$$\Psi = \frac{\partial \eta}{\partial \Theta^T} \quad (31)$$

The Jacobian matrix given in Equation (31) can be obtained by perturbing the design variables  $\Theta$  one at a time and calculating the resultant change in the thermal performance factor  $\eta$  from the solution of direct problems.

To yield an expression for suitable iterative calculation, Equation (27) is rearranged and expressed as:

$$\Theta^{n+1} = \Theta^n + (\Psi^T \Psi + \mu^n \mathbf{I})^{-1} \Psi^T (\eta - \phi) \quad (32)$$

In the beginning, the steepest-descent method ( $\eta^n \rightarrow \infty$ ) is applied, then the value of  $\mu^n$  decreases, and eventually Newton's method ( $\mu^n = 0$ ) is utilized to compute the optimal solutions [13]. A sequence of direct problems is solved by CFD-ACE+ to update the design variables for PTHE-ZR by minimizing the difference between  $\eta$  and  $\phi$  in this optimization algorithm.

## 5. Computational Steps

The iteration steps for obtaining the optimal design variables of this work are summarized below:

- Step 1: Use the original design variables  $\Theta^0$  as the initial guesses to begin the calculations.  
 Step 2: Solve the direct problems and then the estimated  $\eta$  can be obtained from Equation (16).  
 Step 3: The Jacobian matrix is computed with Equation (31).  
 Step 4: Update  $\Theta^{n+1}$  from Equation (32).  
 Step 5: If  $(|J^{n+1} - J^n|/J^{n+1}) < \varepsilon$  is not satisfied, return to Step 2 and repeat.

## 6. Results and Discussion

The optimal design algorithm with LMM was considered in the present study to estimate the design variables of the ribs for the internal Z-shape lateral fins in PTHE-ZR. To illustrate the algorithm of LMM in estimating the design variables of the lateral ribs by minimizing the cost function of PTHE-ZR, the optimal shape design problem is described below.

Copper with the thermal conductivity  $k = 387 \text{ W/(m} \cdot \text{K)}$  was chosen for PTHE-ZR materials and the working conditions were the same as those given by Wang et al. [8]. In addition, the temperature-dependent physical properties of air were identical to those reported by Duan et al. [9].

It is important to verify the accuracy of the computed numerical data because it plays a critical role in the shape design problem. If the solutions obtained by CFD-ACE+ are not accurate enough, the optimal rib dimensions of PTHE-ZR cannot be designed properly and correctly. The following benchmark model is utilized for the above-mentioned purpose, and the numerical results will be compared with the corrected results given by Wang et al. [8].

The geometry for PTHE-Z is illustrated in Figure 1 and is considered as the initial design of this study. Based on Equation (16), the thermal performance factor of PTHE-Z is taken as  $\eta = 1.0$  and the following dimensions are adopted:

- $d_o = 16 \text{ mm}$ ,  $D_i = 32 \text{ mm}$ ,  $D_o = 35 \text{ mm}$ ,  $T_w = 303 \text{ K}$ ,  $T_{in} = 373 \text{ K}$ ,
- $P_{in} = 0.2 \text{ MPa}$ ,  $k_{\text{copper}} = 387 \text{ W/m} \cdot \text{K}$ ,  $\delta = 0.2 \text{ mm}$ ,  $t = 0.1 \text{ mm}$ ,
- $L = 7.6 \text{ mm}$ ,  $L_t = 400 \text{ mm}$ ,  $N = 20$

The volume of each internal Z-type lateral fin can be obtained as  $\text{Vol} = L \times \delta \times L_t = 608 \text{ mm}^3$ . Additionally, temperature-dependent physical properties of air, Equations (7)–(10), were utilized.

The average outlet air temperature of PTHE-Z,  $T_{out}$ , was calculated utilizing CFD-ACE+ package with four different grid numbers 158,400, 323,400, 653,400 and 983,400 at  $\text{Re} = 5000$ , and the computed results were obtained as  $T_{out} = 304.1, 305.6, 306.8$  and  $307.5 \text{ K}$ , respectively. The relative error of  $T_{out}$  between grid numbers 653,400 and 983,400 was calculated as 0.23%, which is very small; thus, grid number 653,400 was considered for all computations in this work.

In addition, in order to verify the necessity for using polynomial temperature-dependent physical properties of air,  $T_{out}$  and  $f$  using constant physical properties measured at  $T = 373 \text{ K}$  (inlet temperature),  $306 \text{ K}$  (outlet temperature) and  $340 \text{ K}$  (averaged temperature), together with utilizing the ideal gas condition were computed with different  $\text{Re}$  values, and the results were then compared with those using polynomial physical properties and the corrected equations reported by Wang et al. [8].

Figure 7a,b illustrates the comparisons of  $T_{out}$  and  $f$  among six cases. Figure 7a indicates that at higher  $Re$ , the values of  $T_{out}$  obtained by using polynomial temperature-dependent physical properties of air matched best with corrected results and Figure 7b shows that the values of  $f$  obtained by using polynomial properties of air always best fit with corrected results. The validity of using temperature-dependent physical properties of air is thus verified. The computed temperature and pressure distributions of PTHE-Z at  $z = 100$  mm are plotted in Figures 8a and 9a, respectively.

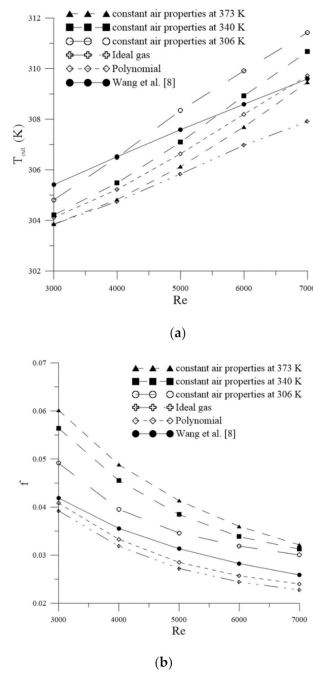


**Figure 7.** The comparisons of (a)  $T_{out}$  and (b)  $f$  for PTHE-Z with the corrected values [8] using five different physical properties of air.

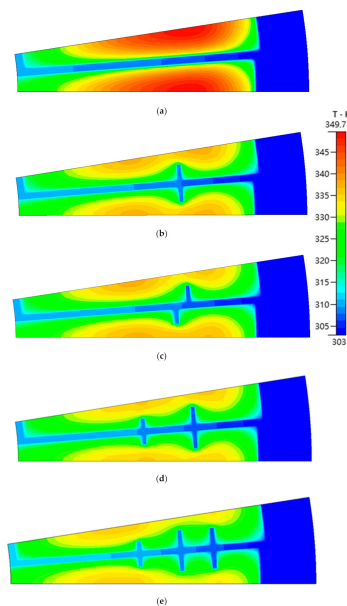


**Figure 8.** The comparisons of temperature distributions for (a) PTHE-Z, (b) design A (c) design B (d) design C and (e) design D at  $z = 100$  mm.

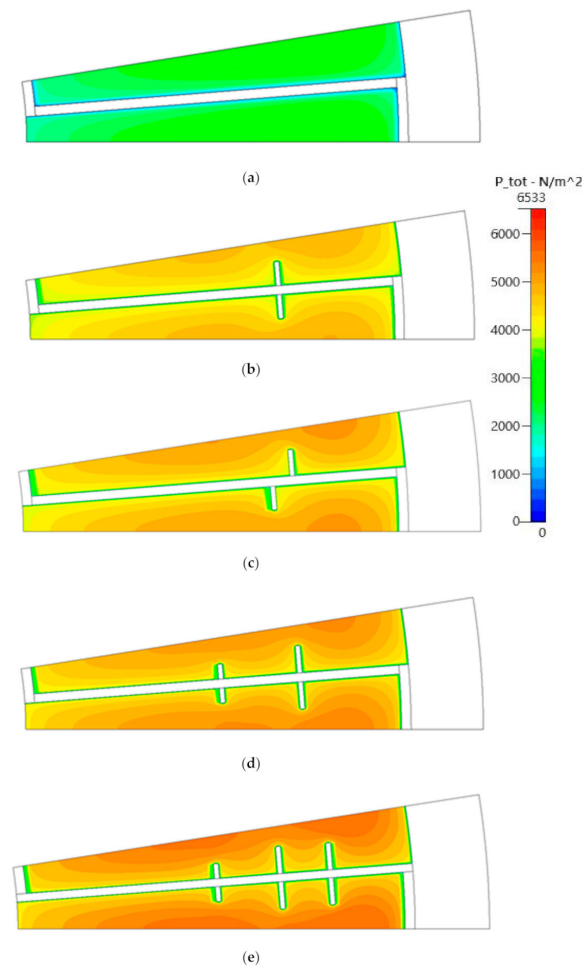


**Figure 9.** The comparisons of pressure distributions for (a) PTHE-Z, (b) design A (c) design B (d) design C and (e) design D at  $z = 100$  mm.

### 6.1. Optimal Design of PTHE-ZR

The objective of the present study was to examine whether the use of lateral ribs can further improve  $\eta$  of the PTHE-Z. A 20% increase in  $\eta$  from PTHE-Z was required, i.e.,  $\varphi = 1.2$ . After executing the design algorithm, it was difficult to reach this desired  $\varphi$  value; however, the optimal design variables could still be obtained for maximum  $\eta$  by using the LMM. The following four design cases were investigated in sequence to identify the most effective design pattern. The stopping criterion  $\varepsilon = 10^{-5}$  and volume of fin and ribs  $\text{Vol} = 608 \text{ mm}^3$  were adopted in this study.

### 6.2. Design A

In design A, it is assumed that there is one pair of ribs and the upper and lower ribs have same position and height, i.e., the design variables are considered as  $W$  and  $H$ . The initial guesses were taken as  $W = 4.50 \text{ mm}$  and  $H = 0.3 \text{ mm}$ , by considering  $\text{Re} = 5000$ ,  $\varphi = 1.2$  and  $\varepsilon = 10^{-5}$ , and after five iterations the estimated design variables were obtained as  $W = 5.16 \text{ mm}$  and  $H = 0.516 \text{ mm}$ , and the fin thickness reduced to  $\eta = 0.18641 \text{ mm}$ . In addition,  $\text{Nu}$ ,  $f$  and  $\eta$  were calculated as 148.4, 0.046 and 1.13, respectively, and are listed in Table 1. The computed temperature and pressure distributions at  $z = 100 \text{ mm}$  are plotted in Figures 8b and 9b, respectively.

**Table 1.** Design variables and optimal results of PTHE-ZRs with various Re.

Design Cases	Design Variables (mm)	Re = 3000			Re = 5000 (Design Condition)			Re = 7000		
		Nu	f	$\eta$	Nu	f	$\eta$	Nu	f	$\eta$
PTHE-Z	N/A	94.2	0.0320	1	112.0	0.0285	1	124.4	0.0240	1
Case A of PTHE-ZR	$W = 5.16, h = 0.516$ $\delta = 0.18641$	118.1	0.0605	1.0990	148.4	0.0460	1.1300	166.5	0.0382	1.1462
Case B of PTHE-ZR	$W_1 = 5.01, h_1 = 0.50$ $W_2 = 5.44, h_2 = 0.55$ $\delta = 0.18623$	118.8	0.0614	1.0998	150.0	0.0472	1.1321	169.1	0.0395	1.1516
Case C of PTHE-ZR	$W_1 = 3.90, h_1 = 0.31$ $W_2 = 5.54, h_2 = 0.57$ $\delta = 0.17682$	122.2	0.0651	1.1097	153.0	0.0498	1.1343	172.1	0.0416	1.1518
Case D of PTHE-ZR	$W_1 = 3.85, h_1 = 0.31$ $W_2 = 5.13, h_2 = 0.56$ $W_3 = 6.14, h_3 = 0.55$ $\delta = 0.16274$	123.9	0.0706	1.0952	154.3	0.0539	1.1147	173.7	0.0453	1.1294

It is clear from Figure 8a,b that by utilizing one pair of lateral ribs in PTHE-ZR, heat dissipation ability in PTHE-ZR is greatly improved than in PTHE-Z, as a result, temperature distribution in Figure 8b is observed lower than that in Figure 8a and therefore Nu of PTHE-ZR is obtained higher than that of PTHE-Z. It is also observed that the optimal position of the ribs of PTHE-ZR is located approximately at the position with the highest air temperature in the upper and lower zones of PTHE-Z. Utilizing intruded cool ribs into the hottest region of air will definitely reduce the average temperature of air effectively.

Due to the added surface area of the ribs, the pressure distribution of PTHE-ZR given in Figure 9b is found to be higher than that of PTHE-Z given in Figure 9a. Therefore, the computed friction  $f$  of PTHE-ZR is larger than that of PTHE-Z. However, when considering the objective function of this study, i.e., to maximize the thermal performance factor  $\eta$ , it is calculated as  $\eta = 1.13$  with the present optimal design shape of ribs, i.e.,  $\eta$  of PTHE-ZR is 13% higher than that of PTHE-Z under fixed fin volume constraint. It verifies that the design concept of this work is correct.

### 6.3. Design B

In design A, it was found that there is a significant increase in  $\eta$  by considering one pair of rib with identical position and height. In design B the upper and lower ribs can have different positions,  $W_1$  and  $W_2$ , and heights,  $H_1$  and  $H_2$ , and hope that  $\eta$  can be increased further.

The design variables are now considered as  $\Theta = \{W_1, H_1, W_2, H_2\}$ . The optimal design variables of design A is used as the initial guesses of design B, i.e.,  $W_1^0 = W_2^0 = 5.16$  mm and  $H_1 = H_2 = 0.516$  mm. By performing the LMM, the optimal solutions can be obtained as  $W_1 = 5.01$  mm,  $W_2 = 5.44$  mm,  $H_1 = 0.50$  mm, and  $H_2 = 0.55$  mm after four iterations, and the fin thickness is obtained as  $\delta = 0.18623$  mm. The resultant characteristics are obtained as  $Nu = 150$ ,  $f = 0.0472$  and  $\eta = 1.1321$ . The calculated temperature and pressure distributions at  $z = 100$  mm are plotted in Figures 8c and 9c, respectively, and the data are summarized in Table 1. It is clear from Figure 8b,c that temperature distributions of design B PTHE-ZR are lower than those of design A PTHE-ZR, due to the flexibility of the designing positions and heights of upper and lower ribs.

It is found that (1)  $W_1$  and  $W_2$  move to the left and right sides from the initial position, respectively, and (2)  $H_1$  and  $H_2$  become shorter and longer than the initial height, respectively, to yield better thermal performance factor  $\eta$ .

The reason for the first observation is that due to structure asymmetry, the hottest region of the lower passage is located left-hand-side of the upper passage. In design A, the positions of upper and lower ribs are identical, therefore the optimal position  $W$  is located approximately between the hottest regions of upper and lower passage. In design B,  $W_1$  and  $W_2$  are estimated by LMM separately to

result in the best heat dissipation performance, and therefore  $W_1$  and  $W_2$  move to the hottest regions of lower and upper passages, respectively. In addition, the vertical distance of the hottest point of the upper passage to the internally lateral fin is greater than that of the lower passage, and as a result,  $H_2$  should be estimated higher than  $H_1$ , and that is the explanation of the second observation.

In design B,  $Nu$  and  $f$  are both increased when compared with design A and the improvement of thermal performance factor  $\eta$  is not significant because it is calculated as  $\eta = 1.1321$  with the estimated optimal design shape of ribs, i.e.,  $\eta$  of design B PTHE-ZR is 13.21% higher than that of PTHE-Z under fixed fin volume constraint, but only 0.21% higher than that in design A.

#### 6.4. Design C

Two pairs of ribs were considered in design C and the position and height of ribs in each pair were assumed to be identical. Figure 5c plots the geometry of the design, i.e., the design variables are taken as  $\Theta = \{W_1, H_1, W_2, H_2\}$ .

The initial guesses of design C are assumed as  $\Theta^0 = \{1.52, 0.30, 4.65, 0.3\}$ . By performing the LMM, after four iterations the optimal solutions can be obtained as  $W_1 = 3.90$  mm,  $W_2 = 5.54$  mm,  $H_1 = 0.31$  mm,  $H_2 = 0.57$  mm and  $\eta = 0.17682$  mm. The resultant characteristics are obtained as  $Nu = 153$ ,  $f = 0.0498$  and  $\eta = 1.1343$ . The calculated temperature and pressure distributions at  $z = 100$  mm are plotted in Figures 8d and 9d, respectively, and the data are summarized in Table 1.

Figure 8d indicates that the second pair of ribs is located at the original hottest region and the first pair of ribs is located at the resultant second hottest region to enhance heat dissipation performance, and the height of ribs in the second pair is higher than that in the first pair for the same reason stated previously. In design C,  $Nu$  and  $f$  are both increased when compared with design B, again the improvement of  $\eta$  is not significant because it is 13.43% higher than that of PTHE-Z under fixed fin volume constraint, but only 0.43% higher than that in design B.

The comparisons among PTHE-Z and PTHE-ZRs indicate that  $\eta$  of the PTHE-ZRs can be improved significantly, however, by varying rib positions and heights and increasing number of ribs from case A to B and to C,  $\eta$  is improved gradually but insignificantly from designs A to B and to C.

Can  $\eta$  be further increased by increasing number of pair of ribs? To answer this, the following design D needs be examined.

#### 6.5. Design D

Three pairs of ribs were utilized in design D and the position and height of ribs in each pair were assumed to be identical. Figure 6c plots the geometry of the design, i.e., the design variables are taken as  $\Theta = \{W_1, H_1, W_2, H_2, W_3, H_3\}$ .

The initial guesses of design D are assumed as  $\Theta^0 = \{3.90, 0.31, 5.54, 0.57, 6.50, 0.57\}$ . By performing the LMM, after three iterations, the optimal solutions can be obtained as  $W_1 = 3.85$  mm,  $W_2 = 5.13$  mm,  $W_3 = 6.14$  mm,  $H_1 = 0.31$ ,  $H_2 = 0.56$  mm,  $H_3 = 0.55$  mm, and  $\delta = 0.16274$  mm. The resultant characteristics are obtained as  $Nu = 154.3$ ,  $f = 0.0539$  and  $\eta = 1.1147$ . The calculated temperature and pressure distributions at  $z = 100$  mm are plotted in Figures 8e and 9e, respectively, and the data are summarized in Table 1.

Figures 8e and 9e illustrate that utilizing three pairs of ribs can enhance heat dissipation but also increase pressure drop. The calculated thermal performance factor  $\eta$  is even smaller than that in design A, which implies that in design D the increase in the enhancement ratio of  $(Nu_{ZR}/Nu_Z)(f_Z/f_{ZR})^{-1/3}$  is smaller than that in design A, and it can be concluded that more pairs of ribs cannot guarantee a higher thermal performance factor  $\eta$ .

The complete cross-sectional view of temperature and pressure distributions for various designs at  $z = 100$  mm are illustrated in Figure 10. It is obvious from Figure 10 that temperatures are decreasing (i.e.,  $Nu$  values are increasing) and pressures are increasing (i.e.,  $f$  values are increasing) monotonically from PTHE-Z to design D. However, with regards to the concern of  $\eta$ , it shows that the  $\eta$  of design D is the smallest among four designs of PTHE-ZR and there is no significant difference of  $\eta$  among

designs A, B and C. Due to manufacturing costs consideration, simpler fin structures are preferred, therefore design A is recommended for practical engineering applications.

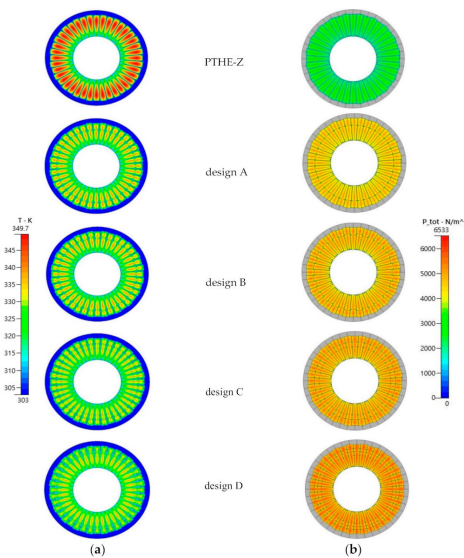


**Figure 10.** The comparisons of cross-sectional view of (a) temperature and (b) pressure distributions for various designs at  $z = 100$  mm.

### 6.6. Hydro-Thermal Characteristics of PTHE-ZRs at $Re = 3000$ and $7000$

Next, the computed values of  $Nu$ ,  $f$  and  $\eta$  of the above PTHE-Z and designed PTHE-ZRs with  $Re = 3000$  and  $7000$  are summarized in Table 1. The variations in  $Nu$ ,  $f$  and  $\eta$  with  $Re$  for various designs are plotted in Figure 11a–c, respectively. As expected,  $Nu$  and  $f$  both increase as rib number increases, and designs C and D have the largest and smallest  $\eta$  among PTHE-ZRs, respectively. Again,  $\eta$  for optimal designs A to D are all greater than 1.0 for the tested range of  $Re$ . This implies that when PTHE-ZRs are not working at the design condition  $Re = 5000$ , the hydro-thermal characteristics are still similar to those working at the design condition.

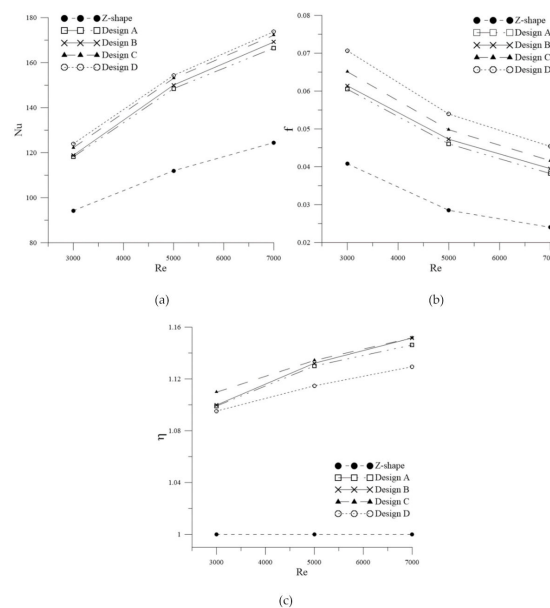


**Figure 11.** The variations of (a)  $Nu$ , (b)  $f$  and (c)  $\eta$  with  $Re$  for various designs.

Finally, it is concluded that the validity of the optimal design for PTHE-ZR has been demonstrated, and this technology can readily be utilized in heat exchanger designs. In addition, wavy-shape fins may have better heat dissipation performance than straight fins, and the determination of optimal internal wavy-shape lateral fins can thus be investigated in the future.

## 7. Conclusions

An inverse shape design problem for pipe type heat exchangers was investigated in this work to determine the optimal shape of continuous lateral ribs on internal Z-shape lateral fins for maximum  $\eta$  with LMM and CFD-ACE+. The validity of using temperature-dependent polynomial function of air properties were verified by comparing the computed  $T_{out}$  and  $f$  with the corrected solutions [8], then four design cases at working condition  $Re = 5000$  were considered based on various positions, heights and numbers of continuous lateral ribs. Results indicated that by considering lateral ribs on the surface of Z-shape lateral fins,  $Nu$  and  $f$  both increase as the number of ribs increase; however, this is not the case for  $\eta$ . The improvements of  $\eta$  in designs A to C PTHE-ZRs (i.e., with two to four ribs) is about 13% higher than that of PTHE-Z, however, is only 11.5% higher in design D. This implies that more ribs will not guarantee a higher  $\eta$  value. In addition, the values of  $\eta$  for designs A, B and C are approximately the same, due to the fact that simpler fin structures lead to lower manufacturing costs, therefore, design A is the best design for industrial applications. Finally, the hydro-thermal characteristics for off-design working conditions at  $Re = 3000$  and  $7000$ , which are not the design conditions, were considered and  $Nu$ ,  $f$  and  $\eta$  were computed. Results revealed that the trends of  $Nu$ ,  $f$  and  $\eta$  at  $Re = 3000$  and  $7000$  are similar to those working at the design condition  $Re = 5000$ . This indicates that the optimal shapes of continuous lateral ribs can be utilized at off-design conditions.

**Author Contributions:** Conceptualization, C.-H.H.; methodology, C.-H.H.; software, C.-Y.K.; validation, C.-H.H. and C.-Y.K.; formal analysis, C.-H.H. and C.-Y.K.; investigation, C.-H.H. and C.-Y.K.; writing—original draft preparation, C.-H.H. and C.-Y.K.; writing—review and editing, C.-H.H.; visualization, C.-Y.K.; supervision, C.-H.H.; project administration, C.-H.H.; funding acquisition, C.-H.H. All authors have read and agreed to the published version of the manuscript.

**Funding:** This work was supported in part through the Ministry of Science and Technology, Taiwan (TW), Grant number, MOST-109-2221-E-006-048-MY3.

**Conflicts of Interest:** The authors declare no conflict of interest.

## Nomenclature

A	total heat transfer area ( $\text{mm}^2$ )
$C_p(T_a)$	specific heat capacity of air ( $\text{kJ/kg-K}$ )
$D_h$	hydraulic diameter
$f$	friction factor
$h$	heat transfer coefficient ( $\text{W/m}^2\text{-K}$ )
H	height of rib (mm)
J	the cost function
$k_a(T_a)$	thermal conductivity of air ( $\text{W/m-K}$ )
L	tube length with fins (mm)
$L_t$	fin length (mm)
N	number of waves
$Nu$	Nusselt number
Re	Reynolds number
t	rib thickness (mm)
$T_s$	solid material temperature (K)
$T_a$	air temperature (K)
$T_w$	wall temperature (K)

$T_{in}$	inlet air temperature (K)
$T_{out}$	outlet air temperature (K)
Vol	volume of fins and ribs ( $\text{mm}^3$ )
W	rib position (mm)
Greek symbols	
$\Omega$	computational domain
$\Theta$	design variable
$\Psi$	Jacobian matrix
$\phi$	desired thermal performance factor
$\delta$	fin thickness (mm)
$\rho(T_a)$	air density ( $\text{kg/m}^3$ )
$\mu$	weighting coefficient
$\mu_i(T_a)$	air dynamic viscosity ( $\text{kg/m-s}$ )
$\eta$	thermal performance factor
$\varepsilon$	stopping criterion
$\Delta P$	pressure drop (Pa)
$\Delta T_{LMTD}$	logarithmic mean temperature difference (K)

## References

- Webb, R.L. *Principles of Enhanced Heat Transfer*; John Wiley & Sons, Inc.: New York, NY, USA, 1994.
- Fabbri, G. Heat transfer optimization in internally finned tubes under laminar flow conditions. *Int. J. Heat Mass Transf.* **1998**, *41*, 1243–1253. [[CrossRef](#)]
- Fabbri, G. Optimum profiles for asymmetrical longitudinal fins in cylindrical ducts. *Int. J. Heat Mass Transf.* **1999**, *42*, 511–523. [[CrossRef](#)]
- El-Sayed, S.A.; EL-Sayed, S.A.; Abdel-Hamid, M.E.; Sadoun, M.N. Experimental study of turbulent flow inside a circular tube with longitudinal interrupted fins in the stream wise direction. *Exp. Therm. Fluid Sci.* **1997**, *15*, 1–15. [[CrossRef](#)]
- Al-Sarkhi, A.; Abu-Nada, E. Characteristics of forced convection heat transfer in vertical internally finned tube. *Int. Commun. Heat Mass Transf.* **2005**, *32*, 557–564. [[CrossRef](#)]
- Wang, Q.; Lin, M.; Zeng, M.; Tian, L. Investigation of Turbulent Flow and Heat Transfer in Periodic Wavy Channel of Internally Finned Tube with Blocked Core Tube. *J. Heat Transf.* **2008**, *130*, 061801. [[CrossRef](#)]
- Yu, B.; Tao, W.-Q. Pressure drop and heat transfer characteristics of turbulent flow in annular tubes with internal wave-like longitudinal fins. *Heat Mass Transf.* **2004**, *40*, 643–651. [[CrossRef](#)]
- Wang, Q.; Lin, M.; Zeng, M. Effect of lateral fin profiles on turbulent flow and heat transfer performance of internally finned tubes. *Appl. Therm. Eng.* **2009**, *29*, 3006–3013. [[CrossRef](#)]
- Duan, L.; Ling, X.; Peng, H. Flow and heat transfer characteristics of a double-tube structure internal finned tube with blossom shape internal fins. *Appl. Therm. Eng.* **2018**, *128*, 1102–1115. [[CrossRef](#)]
- Chai, L.; Xia, G.; Zhou, M.; Li, J.; Qi, J. Optimum thermal design of interrupted microchannel heat sink with rectangular ribs in the transverse microchambers. *Appl. Therm. Eng.* **2013**, *51*, 880–889. [[CrossRef](#)]
- Xia, G.; Zhai, Y.; Cui, Z. Numerical investigation of thermal enhancement in a micro heat sink with fan-shaped reentrant cavities and internal ribs. *Appl. Therm. Eng.* **2013**, *58*, 52–60. [[CrossRef](#)]
- Ahmed, H. Optimization of thermal design of ribbed flat-plate fin heat sink. *Appl. Therm. Eng.* **2016**, *102*, 1422–1432. [[CrossRef](#)]
- Marquardt, D.W. An Algorithm for Least-Squares Estimation of Nonlinear Parameters. *J. Soc. Ind. Appl. Math.* **1963**, *11*, 431–441. [[CrossRef](#)]
- Chen, P.F.; Huang, C.H. An Inverse Hull Design Problem in Optimizing the Desired Wake of Ships. *J. Ship Res.* **2002**, *46*, 138–147.
- Huang, C.-H.; Li, Y.-Y. A three-dimensional shape design problem in determining the boundary geometry to yield isotherms. *Numer. Heat Transf. Part A Appl.* **2019**, *76*, 517–532. [[CrossRef](#)]
- Huang, C.-H.; Chen, M.-H. An estimation of the optimum shape and perforation diameters for pin fin arrays. *Int. J. Heat Mass Transf.* **2019**, *131*, 72–84. [[CrossRef](#)]
- Huang, C.-H.; Tung, P.-W. Numerical and experimental studies on an optimum Fin design problem to determine the deformed wavy-shaped heat sinks. *Int. J. Therm. Sci.* **2020**, *151*, 106282. [[CrossRef](#)]

18. ESI-CFD Inc. CFD-RC User's Manual. Available online: <https://myesi.esi-group.com/downloads/software-documentation/ace-suite-2020.5-user-guide-cfd-viscart-online> (accessed on 1 November 2020).
19. Yang, Y.-T.; Peng, H.-S. Numerical study of the heat sink with un-uniform fin width designs. *Int. J. Heat Mass Transf.* **2009**, *52*, 3473–3480. [[CrossRef](#)]
20. Rahimi, M.; Shabaniyan, S.R.; Alsairafi, A.A. Experimental and CFD studies on heat transfer and friction factor characteristics of a tube equipped with modified twisted tape inserts. *Chem. Eng. Process. Process Intensif.* **2009**, *48*, 762–770. [[CrossRef](#)]
21. Eiamsaard, P.; Piriyaungroj, N.; Thianpong, C. A case study on thermal performance assessment of a heat exchanger tube equipped with regularly-spaced twisted tapes as swirl generators. *Case Stud. Therm. Eng.* **2014**, *3*, 86–102. [[CrossRef](#)]

**Publisher's Note:** MDPI stays neutral with regard to jurisdictional claims in published maps and institutional affiliations.



© 2020 by the authors. Licensee MDPI, Basel, Switzerland. This article is an open access article distributed under the terms and conditions of the Creative Commons Attribution (CC BY) license (<http://creativecommons.org/licenses/by/4.0/>).